



## Non-invasive Early Response Monitoring of Nanoparticle-assisted Photothermal Cancer Therapy Using $^{18}\text{F}$ -FDG, $^{18}\text{F}$ -FLT, and $^{18}\text{F}$ -FET PET/CT Imaging

Jørgensen, Jesper Tranekjær; Nørregaard, Kamilla; Simon Martin, Marina; Oddershede, Lene Broeng; Kjær, Andreas

*Published in:*  
Nanotheranostics

*DOI:*  
[10.7150/ntno.24478](https://doi.org/10.7150/ntno.24478)

*Publication date:*  
2018

*Document version*  
Publisher's PDF, also known as Version of record

*Citation for published version (APA):*  
Jørgensen, J. T., Nørregaard, K., Simon Martin, M., Oddershede, L. B., & Kjær, A. (2018). Non-invasive Early Response Monitoring of Nanoparticle-assisted Photothermal Cancer Therapy Using  $^{18}\text{F}$ -FDG,  $^{18}\text{F}$ -FLT, and  $^{18}\text{F}$ -FET PET/CT Imaging. *Nanotheranostics*, 2(3), 201-210. <https://doi.org/10.7150/ntno.24478>

## Research Paper

# Non-invasive Early Response Monitoring of Nanoparticle-assisted Photothermal Cancer Therapy Using $^{18}\text{F}$ -FDG, $^{18}\text{F}$ -FLT, and $^{18}\text{F}$ -FET PET/CT Imaging

Jesper Tranekjær Jørgensen<sup>1,\*</sup>, Kamilla Norregaard<sup>1,\*</sup>, Marina Simón Martín<sup>1</sup>, Lene Broeng Oddershede<sup>2</sup>, Andreas Kjaer<sup>1</sup>✉

1. Cluster for Molecular Imaging, Dept. of Biomedical Sciences and Department of Clinical Physiology, Nuclear Medicine & PET, Rigshospitalet and University of Copenhagen, Denmark
2. Niels Bohr Institute, University of Copenhagen, Denmark

\*Contributed equally

✉ Corresponding author: A. K. (akjaer@sund.ku.dk)

© Ivyspring International Publisher. This is an open access article distributed under the terms of the Creative Commons Attribution (CC BY-NC) license (<https://creativecommons.org/licenses/by-nc/4.0/>). See <http://ivyspring.com/terms> for full terms and conditions.

Received: 2018.01.02; Accepted: 2018.03.21; Published: 2018.04.27

## Abstract

**Rationale:** Since its first implementation nanoparticle-assisted photothermal cancer therapy has been studied extensively, although mainly with focus on optimal nanoparticle design. However, development of efficient treatment protocols, as well as reliable and early evaluation tools *in vivo*, are needed to push the therapy towards clinical translation. Positron emission tomography (PET) is a non-invasive imaging technique that is currently finding extensive use for early evaluation of cancer therapies; an approach that has become of increasing interest due to its great potential for personalized medicine.

**Methods:** In this study, we performed PET imaging to evaluate the treatment response two days after nanoparticle-assisted photothermal cancer therapy in tumor-bearing mice. We used three different tracers; 2'-deoxy-2'- $^{18}\text{F}$ -fluoro-D-glucose ( $^{18}\text{F}$ -FDG), 3'-deoxy-3'- $^{18}\text{F}$ -fluorothymidine ( $^{18}\text{F}$ -FLT), and O-(2'- $^{18}\text{F}$ -fluoroethyl)-L-tyrosine ( $^{18}\text{F}$ -FET) to image and measure treatment induced changes in glucose uptake, cell proliferation, and amino acid transport, respectively. After therapy, tumor growth was monitored longitudinally until endpoint was reached.

**Results:** We found that nanoparticle-assisted photothermal therapy overall inhibited tumor growth and prolonged survival. All three PET tracers had a significant decrease in tumor uptake two days after therapy and these changes correlated with future tumor growth, with  $^{18}\text{F}$ -FDG having the most predictive value in this tumor model.

**Conclusion:** This study shows that  $^{18}\text{F}$ -FDG,  $^{18}\text{F}$ -FLT, and  $^{18}\text{F}$ -FET are all robust markers for the treatment response of photothermal therapy, and demonstrate that PET imaging can be used for stratification and optimization of the therapy. Furthermore, having a selection of PET tracers that can reliably measure treatment response is highly valuable as the individual tracer might be excluded in certain applications where physiological processes limit their contrast to background.

Key words: Photothermal therapy, nanoparticles, PET imaging, response monitoring

## Introduction

Photothermal cancer therapy is a treatment strategy that utilizes light-to-heat converting nanoparticles embedded in the tumor to create local

hyperthermia and ablation by irradiation of near-infrared (NIR) light [1-6]. As the nanoparticles can be designed to be biocompatible and the laser

employed is in the non-phototoxic NIR region, this strategy is thought to be highly target specific with minimal adverse effects. With the perspective of translating photothermal therapy to clinical settings, there is now an increasing need for *in vivo* evaluation of the therapy with the help of companion diagnostics that can be used for early prognosis and treatment optimization.

Traditionally, evaluation of anti-cancer therapeutics has relied on changes in tumor size and burden as readout for therapeutic efficacy [7]. The process of tumor shrinkage/growth can, however, be fairly slow, and changes can often first be detected late after treatment initiation. In addition, tumor size may not reflect efficacy of cancer therapy, e.g. as seen in pseudoprogression during successful immunotherapy. In contrast, positron emission tomography (PET) is a non-invasive molecular imaging technique that provides information on the biological functionality of the tumor based on uptake of a radiolabeled tracer. Changes in tracer uptake after treatment can be used for early response evaluation and to predict treatment outcome, thereby identifying responders from non-responders and facilitating better management of treatment planning [8]. In particular glucose analogue, 2'-deoxy-2'- $^{18}\text{F}$ -fluoro-D-glucose ( $^{18}\text{F}$ -FDG), has been established as a robust tool, based on the high rate of glucose consumption commonly found in cancer cells, for tumor detection, diagnosis, early treatment evaluation, and patient stratification.  $^{18}\text{F}$ -FDG is taken up by cells by the same pathway as glucose but gets trapped after phosphorylation by hexokinase in its first metabolite form, as it cannot undergo further metabolism [9].

Previously, we have shown that  $^{18}\text{F}$ -FDG uptake is significantly reduced after photothermal cancer therapy in human tumor xenografts in mice and can be used as a prognostic marker for the therapeutic outcome [10]. Although imaging with  $^{18}\text{F}$ -FDG shows great promise for early response evaluation of photothermal therapy there are biological limitations to the use of  $^{18}\text{F}$ -FDG that can hamper its specificity. For example, biological processes, such as inflammation, can change the uptake of  $^{18}\text{F}$ -FDG [11, 12]. When inflammation occurs in response to cancer therapy, it can lead to an overestimation in the  $^{18}\text{F}$ -FDG tumor signal due to the increase of activated inflammatory cells in the target tissue [13]. Also there has to be adequate contrast between target and background. This sometimes represents a problem in tumors with inherent low glucose uptake or with tumors where the adjacent tissues have a naturally high glucose turnover, e.g., brain tumors. As a consequence  $^{18}\text{F}$ -FDG imaging is not applicable for all tumor types and is, e.g., in clinic not used routinely

for imaging of brain tumors and prostate cancer [14, 15]. Also the robustness of  $^{18}\text{F}$ -FDG PET for breast cancer is much debated [16, 17].

Apart from glucose consumption, cell proliferation is usually also increased in cancerous tissue and hence may be a better marker to image in cases where  $^{18}\text{F}$ -FDG cannot be used reliably. The tracer 3'-deoxy-3'- $^{18}\text{F}$ -fluorothymidine ( $^{18}\text{F}$ -FLT) is a thymidine analogue that has been successfully used to image cell proliferation *in vivo* [18]. Similar to  $^{18}\text{F}$ -FDG,  $^{18}\text{F}$ -FLT is taken up by the cell where after it is phosphorylated by thymidine kinase 1 and gets trapped intracellularly, thereby visualizing nucleotide transport [19, 20]. However,  $^{18}\text{F}$ -FLT is not incorporated into DNA but is considered a surrogate marker of DNA synthesis. For imaging of brain tumors, where background uptake of  $^{18}\text{F}$ -FDG is high and  $^{18}\text{F}$ -FLT is less valuable as it does not cross the intact blood-brain-barrier, the radiolabelled amino acid analogue O-(2'- $^{18}\text{F}$ -fluoroethyl)-L-tyrosine ( $^{18}\text{F}$ -FET) has been shown to be a good marker [21, 22].  $^{18}\text{F}$ -FET is taken up by the cells via the L-type amino acid transport system, however, it is neither incorporated into proteins nor metabolized. Therefore it is not trapped intracellularly, and consequently  $^{18}\text{F}$ -FET is mainly visualizing amino acid transport rates [23].

All three PET tracers mentioned above have previously been used both pre-clinically and clinically for cancer imaging and treatment evaluation. However, dependent on the mechanism of action induced by the treatment as well as tumor type, one tracer could be more suitable than the others, and selecting the right one could improve the outcome for the individual patient. To our knowledge, so far only  $^{18}\text{F}$ -FDG has been used for PET-based imaging and treatment evaluation of photothermal cancer therapy [10, 24-26]. Therefore, the aim of the study was for the first time to examine the performance of  $^{18}\text{F}$ -FLT and  $^{18}\text{F}$ -FET PET imaging for treatment response evaluation of photothermal cancer therapy in a tumor model in mice and compare it to that of  $^{18}\text{F}$ -FDG.

## Materials and Methods

### Silica-gold nanoshells

Silica-gold nanoshells (NS) consisting of a  $119 \pm 5$  nm diameter silica core surrounded by a 19 nm thick gold shell were obtained from NanoComposix, USA (overall diameter of  $157 \pm 9$  nm). The size of the particle was measured using transmission electron microscopy by the supplier. The maximum absorbance was measured to be 804 nm in water using a UV-visible spectrometer also provided by the supplier.

### Animal model

All animal studies were approved by the Danish

Animal Welfare Council, ministry of Justice. Five weeks old female Balb/c mice (Charles River) were allowed to acclimatize for one week with access to water and chow *ad libitum*. Mouse colon carcinoma cell line (CT26; obtained from ATCC) was cultured in RPMI-1640 medium supplemented with 10% fetal bovine serum and 1% penicillin-streptomycin at 37 °C and 5% CO<sub>2</sub>. Cells were harvested by trypsinization at a confluence of 80-90% and subcutaneous tumors were established in the left flank of the animals by inoculation of  $\sim 3 \times 10^5$  CT26 cells resuspended in 100  $\mu$ l growth media. The tumor growth was followed by caliper measurements and tumor volume calculated as  $\frac{1}{2}(\text{length} \times \text{width}^2)$ . The animals were grouped in three studies representing <sup>18</sup>F-FDG, <sup>18</sup>F-FLT, and <sup>18</sup>F-FET, and within these three groups, three subgroups representing: NS and laser irradiation (NS group); saline and laser irradiation (saline group); or NS but no laser irradiation (sham group). The number of animals in the <sup>18</sup>F-FDG study was:  $n = 7$  (NS group),  $n = 6$  (saline group), and  $n = 7$  (sham group). The number of animals in the <sup>18</sup>F-FLT study was:  $n = 8$  (NS group),  $n = 7$  (saline group), and  $n = 6$  (sham group). The number of animals in the <sup>18</sup>F-FET study was:  $n = 7$  (NS group),  $n = 7$  (saline group), and  $n = 7$  (sham group).

### Photothermal Therapy

Immediately after a baseline PET/CT scan, all animals were injected with 190  $\mu$ l of either  $4.9 \times 10^{10}$  NS/ml or saline via the tail vein while being anesthetized by breathing sevoflurane. 24 hours after intravenous injection of either NS or saline, all animals were again anesthetized by breathing sevoflurane and placed on an irradiation platform with temperature control to maintain their body temperature. The tumors in the NS and saline groups were then irradiated for 5 minutes with an 807 nm diode laser with an intensity of 1.5 W/cm<sup>2</sup> (beam diameter of  $\sim 1$  cm). In addition, animals were injected subcutaneously with  $\sim 70$   $\mu$ l of 0.3 mg/ml of Temgesic (1:9 ratio to sterile water) for pain relief every 6-8 hours for 24 hours after treatment. After treatment, the tumor growth was monitored using caliper measurements and the animals were euthanized when their tumor volume exceeded 1000 mm<sup>3</sup>.

### Thermographic temperature measurements

While being irradiated (or sham treated), the surface temperature of all tumors was measured using thermographic imaging (FLIR T420). Images were recorded every 30 seconds and the maximum temperature as a function of time was extracted by analysis with FLIR tools software.

### PET/CT

All animals were PET/CT scanned the day before laser treatment (baseline scan) and 2 days after treatment (day 2). In addition, they were CT scanned 7 days after treatment. During the entire procedure, animals were anesthetized by breathing sevoflurane and their temperature kept stable with either a heating pad or lamp. As all animals were treated with Temgesic that causes loss of appetite and thereby weight loss, they were not fasted before PET scans. <sup>18</sup>F-FDG, <sup>18</sup>F-FLT, and <sup>18</sup>F-FET were obtained from the daily productions for clinical use at Department of Nuclear Medicine & PET, Rigshospitalet, Denmark. Animals were administered  $\sim 10$  MBq <sup>18</sup>F-FDG or <sup>18</sup>F-FLT via the tail vein 1 hour before the PET scan, or  $\sim 5$  MBq <sup>18</sup>F-FET via the tail vein 30 minutes before the PET scan. In between the <sup>18</sup>F-FDG or <sup>18</sup>F-FET injections and the PET/CT scans, the animals were kept anesthetized. Static PET images were acquired 60-70 min post injection (30-40 min post injection for <sup>18</sup>F-FET) with an energy window of 350-650 KeV and a time resolution of 6 ns. CT scans were acquired using 360 projections, 65 kV, 500  $\mu$ A and 400 ms. PET images were reconstructed using a 3-dimensional maximum a posteriori algorithm with CT-based attenuation correction. PET and CT images were co-registered and analyzed using Inveon software (Siemens). The mean percentage of injected dose per grams of tissue (%ID/g) in the tumor volume was extracted by manually drawing regions of interest on the entire tumor.

### Autoradiography and hematoxylin and eosin (H&E) staining

For each tracer, a NS, saline and sham group ( $n = 3$  in each group) were treated and irradiated according to the above described treatment protocol. At day 2 after treatment, they were injected with tracer via the tail vein while being anesthetized by breathing sevoflurane. One hour after injection (or 30 min for <sup>18</sup>F-FET), the animals were euthanized and the tumors resected. Tumors were immediately frozen by immersion in isopentane and embedded in tissue-tek and when it had solidified, the tumors were sectioned into  $\sim 9$   $\mu$ m slices using a cryostat. The sections were exposed on phosphorous films and imaged on a Cyclone plus imaging system (Perkin Elmer) for visualization of the tracers' intratumoral distribution. Thereafter the sections were dried overnight at room temperature and transferred to -80°C for further analysis.

For H&E staining, frozen sections were left to equilibrate to room temperature for 30 minutes and were subsequently immersed in cold acetone and then in HistoClear solution (Chemie Brunschwig) to

achieve removal of tissue-tek. The sections were then rehydrated through a series of ethanol solutions and transferred to running water. Afterwards, they were stained with hematoxylin for 3 minutes, rinsed in tap water and finally stained with eosin for 1 minute. Slides were scanned with an Axio Scanner (Axio scan, Carl Zeiss, Germany).

### Statistical analysis

The temperature elevation measured on the surface of the tumor with FLIR camera and the mean uptake ratios of the PET tracers were compared with one-way ANOVA with Tukeys post-hoc test. Survival was based on tumor volumes  $\geq 1,000 \text{ mm}^3$  (humane endpoint), and curves were analyzed using Log-rank Mantel-Cox test. The mean and max uptake of PET tracers and mean CT volume in different groups were compared between time points with a two-way ANOVA with Sidak post-hoc test. Statistical analyses were performed using GraphPad Prism 6.

### Results

#### Treatment response to photothermal therapy in vivo using silica-gold nanoparticles as photothermal agents

In this study we used 150 nm in diameter NS as the heat-transducing agent, a class of NIR-absorbing nanoparticles that has been widely used for photothermal therapy in animal studies and has been included in a few FDA-approved clinical trials [27-29].

We have in previous studies made in-depth characterization of the properties and heating capabilities of these NS both as single particles and in bulk [10, 24]. NS have been shown to accumulate passively in tumors upon intravenous administration in several different tumor models [10, 30-34] and to have good treatment effect in the same murine colorectal tumor model as used in this study [6]. Further, toxicology studies show no signs of adverse effects [35, 36].

Each animal was scanned with only one of the PET tracers so the study consisted of three substudies where animals were scanned with either  $^{18}\text{F}$ -FDG,  $^{18}\text{F}$ -FLT, or  $^{18}\text{F}$ -FET before and after treatment (see the experimental timeline in Figure 1A). Within each substudy there were three treatment groups receiving either: NS and laser irradiation (NS group); saline and laser irradiation (saline group); or NS but no laser irradiation (sham group). The latter two groups serve as control groups for the influence of laser irradiation and the NS *per se*, respectively.

Approximately two weeks before the study was initiated, tumors were established subcutaneously in the left flank of female Balb/c mice by inoculation of CT26 cells. Two days before photothermal treatment the mice were grouped so the mean tumor volume, assessed by caliper measurements, was matched for all three groups. Furthermore, the mean tumor volumes in the groups were also kept consistent between the three studies (see Figure 1B).

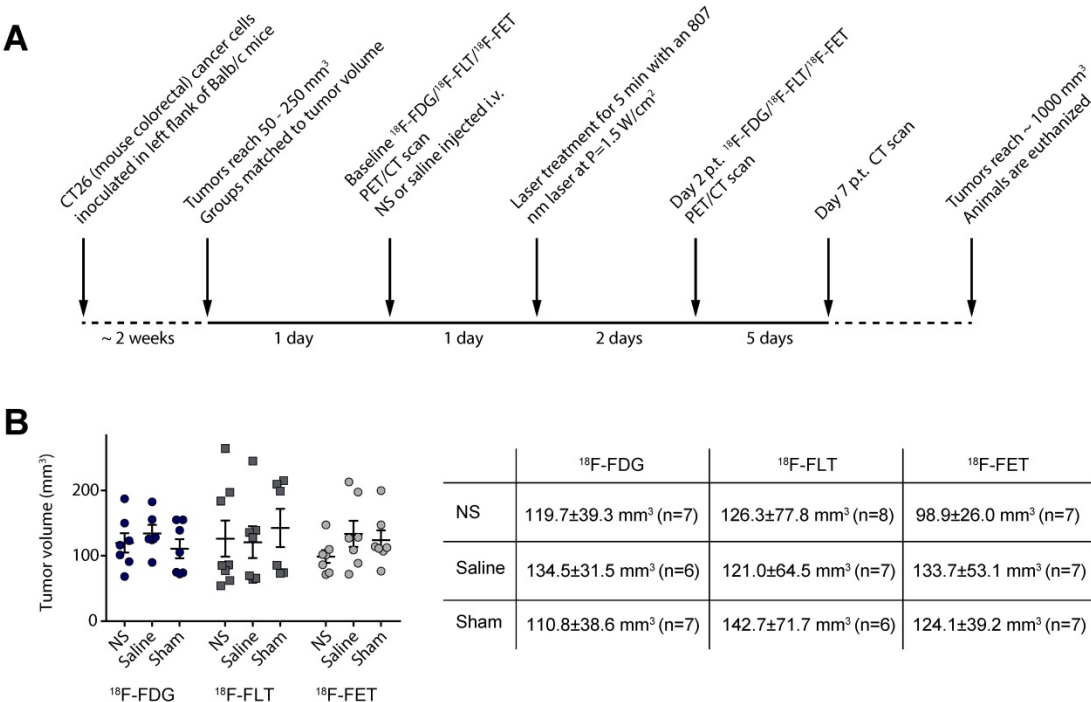


**Figure 1.** Experimental timeline for the study. (A) The experimental setup was the same for all three PET tracers. (B) Graph shows the tumor volume of each individual animal whereas the table shows mean  $\pm$  standard deviation as well as number of animals in each group.



After the baseline PET/CT scan, the animals were injected intravenously with either NS or saline. The nanoparticles were allowed to accumulate for a day, where after the animals were treated for 5 min with a 807 nm diode laser covering the tumor region and using a laser intensity of 1.5 W/cm<sup>2</sup>. Figure 2A shows the average maximum temperature development for all groups during laser irradiation measured using a thermographic camera on the surface of the tumor. In the NS groups the average maximum temperature was 50.6 ± 1.6 °C in the <sup>18</sup>F-FDG study, 49.4 ± 2.0 °C in the <sup>18</sup>F-FLT study, and 52.0 ± 1.5 °C in the <sup>18</sup>F-FET study. In comparison, the average maximum temperature in the saline groups was 43.5 ± 0.4 °C in the <sup>18</sup>F-FDG study, 42.3 ± 0.5 °C in the <sup>18</sup>F-FLT study, and 45.1 ± 0.5 °C in the <sup>18</sup>F-FET study. The average maximum temperatures in the sham groups were all ~31 °C. For all three substudies, the maximum temperature reached in the NS group after 5 min of irradiation was significantly higher than in both the control groups ( $p \leq 0.01$ ).

During the entire study, the tumor growth was followed ~3 times a week using caliper measurements, and when the tumor volumes reached 1,000 mm<sup>3</sup> the animals were euthanized. The study

was terminated at day 60 after therapy, and animals with no tumor regrowth at this time point were considered tumor free. Figure 2B shows that the tumor growth overall was inhibited in animals in the NS group and for all three studies, at least one animal had complete tumor disappearance. In comparison, the tumor growth in the two control groups progressed in a similar manner. This indicates that even though the laser in itself can induce a temperature rise of ~10 °C, as represented in the saline groups, it does not inflict enough tissue damage to inhibit tumor growth.

The survival curves for all three studies are shown in Figure 2C. In the <sup>18</sup>F-FDG study the median survival was 25 days in the NS group, 12 days in the saline group, and 11 days in the sham group. In the <sup>18</sup>F-FLT study the median survival was 24 days in the NS group, 13 days in the saline group, and 13 days in the sham group. And finally, in the <sup>18</sup>F-FET study the median survival was 22 days in the NS group, 15 days in the saline group, and 11 days in the sham group. The survival curves for the different treatment groups were compared with a Log-rank (Mantel-Cox test) with  $p = 0.0099$  in the <sup>18</sup>F-FDG study,  $p = 0.0192$  in the <sup>18</sup>F-FLT study, and  $p < 0.0001$  in the <sup>18</sup>F-FET study.

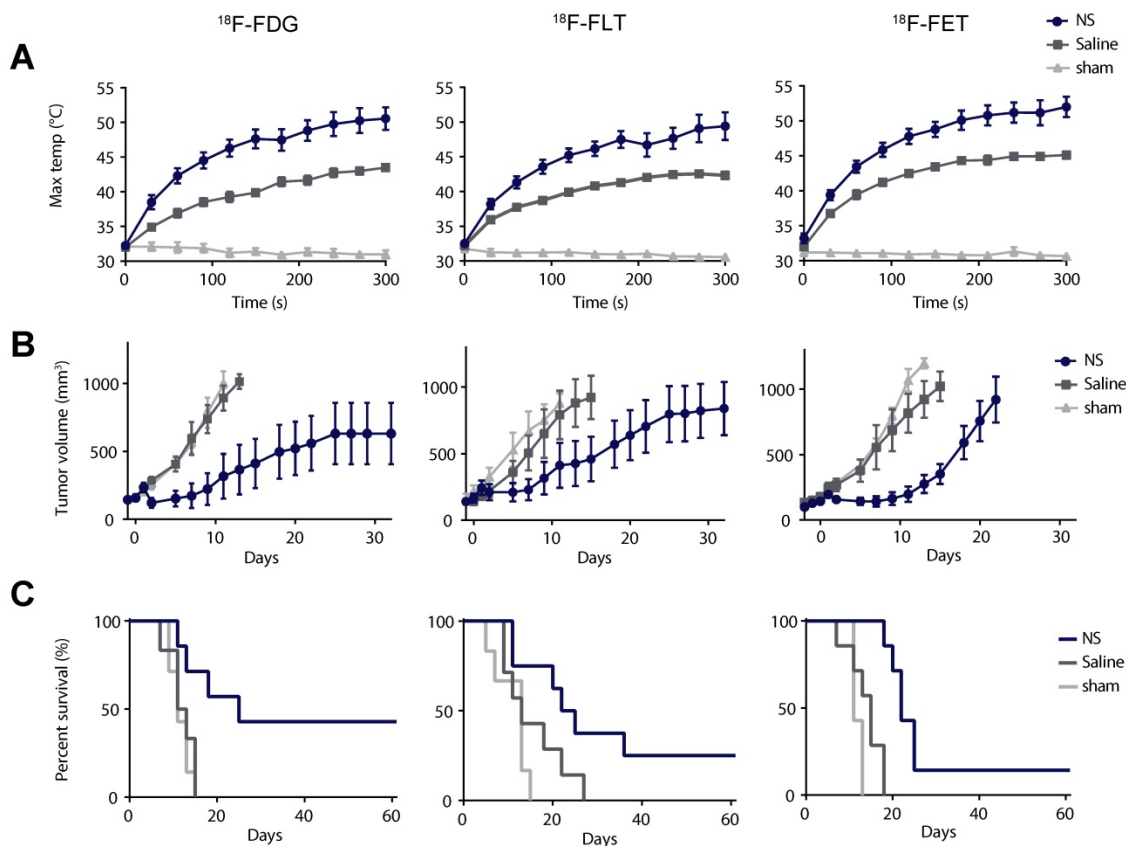


**Figure 2:** Evaluation of photothermal therapy. (A) Thermographic real-time measurements of maximum tumor surface temperature during irradiation. (B) Tumor growth measured after therapy using a caliper. Data is shown until  $n \geq 3$ . (C) Survival after therapy. In (A) and (B) data shown is mean ± standard error of mean (S.E.M). <sup>18</sup>F-FDG:  $n = 7$  (NS group),  $n = 6$  (saline group), and  $n = 7$  (sham group). <sup>18</sup>F-FLT:  $n = 8$  (NS group),  $n = 7$  (saline group), and  $n = 6$  (sham group). <sup>18</sup>F-FET:  $n = 7$  (NS group),  $n = 7$  (saline group), and  $n = 7$  (sham group).

These results show that in all three studies, NS-mediated photothermal therapy inhibited tumor growth and increased survival compared to groups receiving either only laser irradiation (saline group) or NS injections (sham group).

### PET evaluation of photothermal therapy

Visual inspection of PET/CT images revealed no apparent differences in the baseline tumor uptake between treatment groups in the  $^{18}\text{F}$ -FDG,  $^{18}\text{F}$ -FLT, and  $^{18}\text{F}$ -FET study (Figure 3). However, for all three tracers, a reduction in tumor uptake in the NS treated animals was evident between baseline and day 2. This decrease was not observed in animals receiving saline or sham treatment.

These observations were confirmed by quantitative analysis of tracer uptake in 3D ROIs manually drawn on tumor areas (see Figure 4 and extracted values listed in Table 1). For all of the tracers there was no significant difference in the mean tumor uptake at baseline between the three different treatment groups (Figure 4A and Table 1). However, the tumor accumulation of  $^{18}\text{F}$ -FLT showed a larger variation between groups, whereas the mean tumor uptake of  $^{18}\text{F}$ -FET was slightly lower than for  $^{18}\text{F}$ -FDG and  $^{18}\text{F}$ -FLT. Two days after treatment, the mean tumor uptake in the NS treated animals was significantly reduced compared to baseline for all three tracers (Figure 4A and Table 1). This reduction was not seen in sham and saline treated animals.

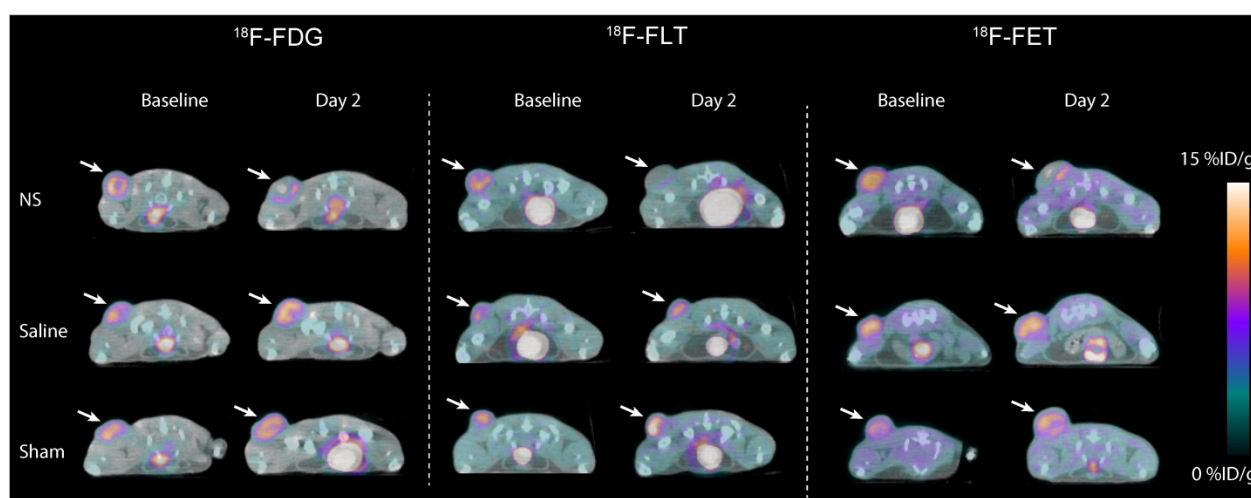


**Figure 3.** Representative images of  $^{18}\text{F}$ -FDG (left panel),  $^{18}\text{F}$ -FLT (middle panel) and  $^{18}\text{F}$ -FET (right panel) tumor uptake the day before photothermal therapy (baseline) and two days after treatment (day 2). Tumors are marked by white arrows.

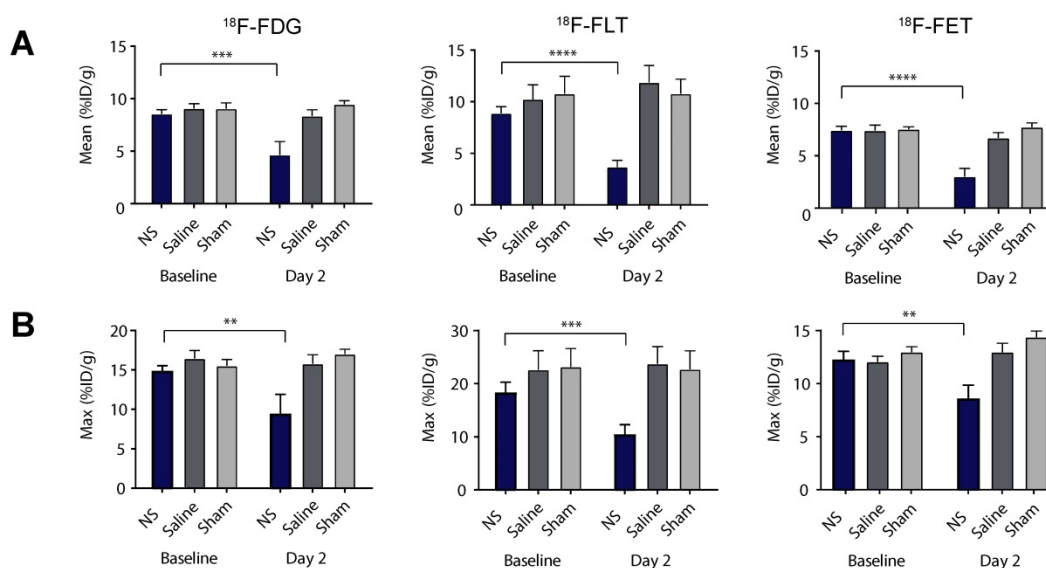


**Figure 4:** Tumor uptake of the PET tracers. (A-B) The mean and maximum PET tracer uptake (%ID/g) at baseline and day 2 for all NS, saline and sham treated animals in the  $^{18}\text{F}$ -FDG (left panel),  $^{18}\text{F}$ -FLT (middle panel) and  $^{18}\text{F}$ -FET (right panel) studies. Data shown is mean  $\pm$  S.E.M and  $^{*}p < 0.01$ ,  $^{***}p < 0.001$ , and  $^{****}p < 0.0001$ .  $^{18}\text{F}$ -FDG:  $n = 7$  (NS group),  $n = 6$  (saline group), and  $n = 7$  (sham group).  $^{18}\text{F}$ -FLT:  $n = 8$  (NS group),  $n = 7$  (saline group), and  $n = 6$  (sham group).  $^{18}\text{F}$ -FET:  $n = 7$  (NS group),  $n = 7$  (saline group), and  $n = 7$  (sham group).

The same trend was found for the maximum tumor uptake, although the changes in accumulation between baseline and day 2 were not as significant (see Figure 4B). Given that photothermal therapy can induce fairly heterogeneous temperatures throughout the tumor, the use of a maximum uptake value, that only carries information about tracer accumulation in a very small portion of the tumor, is likely to be a less robust measure for this type of therapy. Therefore, further analysis was based on the mean uptake only.

Next, we evaluated the mean uptake ratio between day 2 and baseline as a measure of treatment effect (Figure 5A and Table 1). This was found to be significantly lower in all the NS groups compared to the control groups for all tracers. To see if this change in tumor uptake early after therapy could be used as an indicator for treatment outcome we examined the linear correlation between the uptake ratio and survival (see Figure 5B).  $^{18}\text{F}$ -FDG showed the highest correlation to survival ( $r^2=0.62$ ,  $p=0.0001$ ), although all three tracers correlated significantly ( $r^2=0.43$ ,  $p=0.0013$  and  $r^2=0.34$ ,  $p=0.0057$  for  $^{18}\text{F}$ -FLT and  $^{18}\text{F}$ -FET, respectively).

Finally, as change in tumor growth also is commonly used in the clinic to assess treatment effect, we evaluated the tumor volume from CT scans 7 days after therapy (see Figure 5C). This confirmed inhibited tumor growth in the NS groups compared to the two control groups that both had significant increase in tumor volume at day 7 compared to baseline.

**Table 1:** Quantified PET uptake. The table shows the mean tumor uptake on baseline and day 2 and the uptake ratio defined as Day2/Baseline. Values are given as mean  $\pm$  S.E.M.

	Mean uptake	NS	Saline	Sham
$^{18}\text{F}$ -FDG	Baseline (%ID/g)	8.6 $\pm$ 0.4	9.1 $\pm$ 0.5	9.1 $\pm$ 0.6
	Day 2 (%ID/g)	4.7 $\pm$ 1.3	8.4 $\pm$ 0.6	9.5 $\pm$ 0.3
	Ratio (day 2 /baseline)	0.52 $\pm$ 0.14	0.93 $\pm$ 0.07	1.06 $\pm$ 0.05
$^{18}\text{F}$ -FLT	Baseline (%ID/g)	8.9 $\pm$ 0.6	10.2 $\pm$ 1.4	10.8 $\pm$ 1.7
	Day 2 (%ID/g)	3.7 $\pm$ 0.6	11.9 $\pm$ 1.6	10.8 $\pm$ 1.4
	Ratio (day 2 /baseline)	0.41 $\pm$ 0.06	1.21 $\pm$ 0.14	1.03 $\pm$ 0.09
$^{18}\text{F}$ -FET	Baseline (%ID/g)	7.4 $\pm$ 0.4	7.4 $\pm$ 0.5	7.5 $\pm$ 0.2
	Day 2 (%ID/g)	3.0 $\pm$ 0.8	6.7 $\pm$ 0.5	7.7 $\pm$ 0.4
	Ratio (day 2 /baseline)	0.41 $\pm$ 0.11	0.91 $\pm$ 0.06	1.03 $\pm$ 0.06

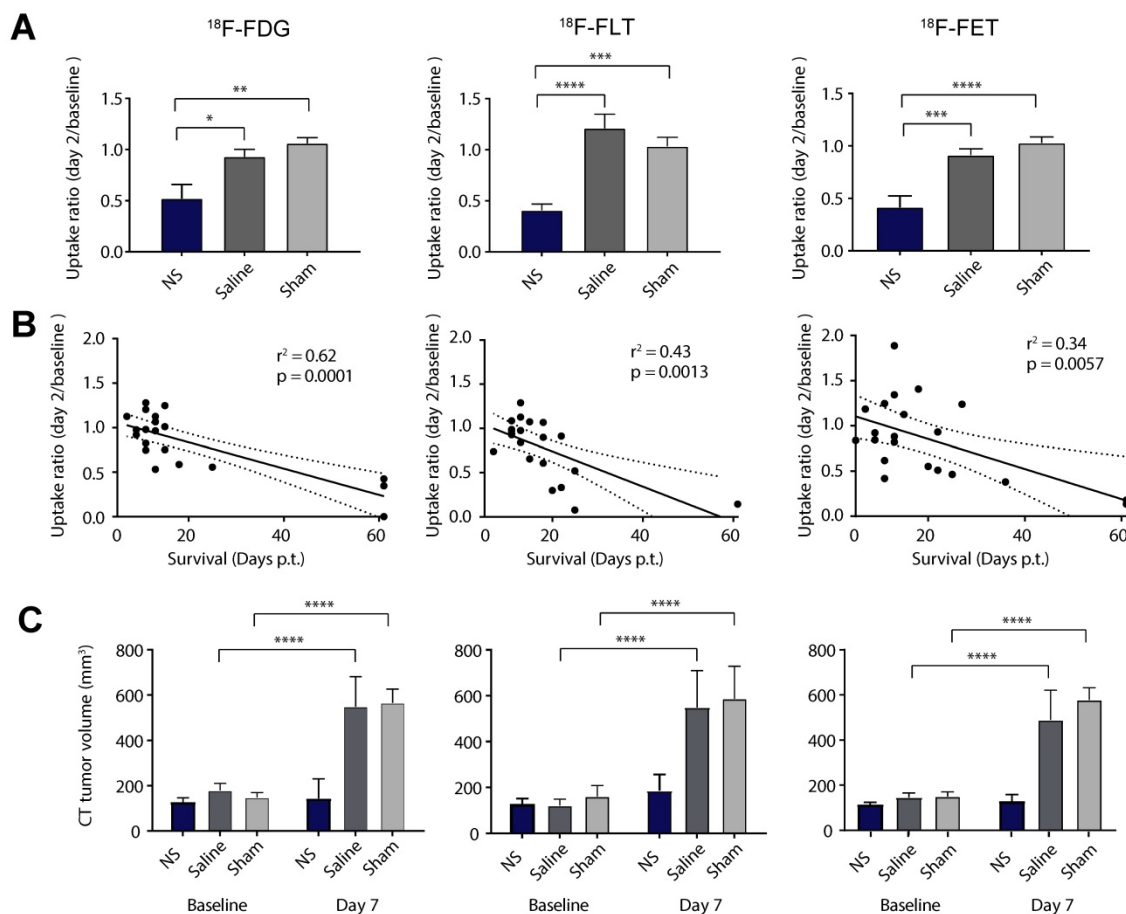


**Figure 5:** PET/CT-based response analysis. (A) The relative change in mean uptake (day2/baseline) for all NS, saline and sham treated animals in the  $^{18}\text{F}$ -FDG (left panel),  $^{18}\text{F}$ -FLT (middle panel) and  $^{18}\text{F}$ -FET (right panel) studies. (B) The correlation between the relative change in uptake and survival. (C) Tumor volumes derived from CT scans at baseline and day 7. Data shown is mean  $\pm$  S.E.M and \* $p < 0.05$ , \*\* $p < 0.01$ , \*\*\* $p < 0.001$ , and \*\*\*\* $p < 0.0001$ .  $^{18}\text{F}$ -FDG:  $n = 7$  (NS group),  $n = 6$  (saline group), and  $n = 7$  (sham group).  $^{18}\text{F}$ -FLT:  $n = 8$  (NS group),  $n = 7$  (saline group), and  $n = 6$  (sham group).  $^{18}\text{F}$ -FET:  $n = 7$  (NS group),  $n = 7$  (saline group), and  $n = 7$  (sham group).



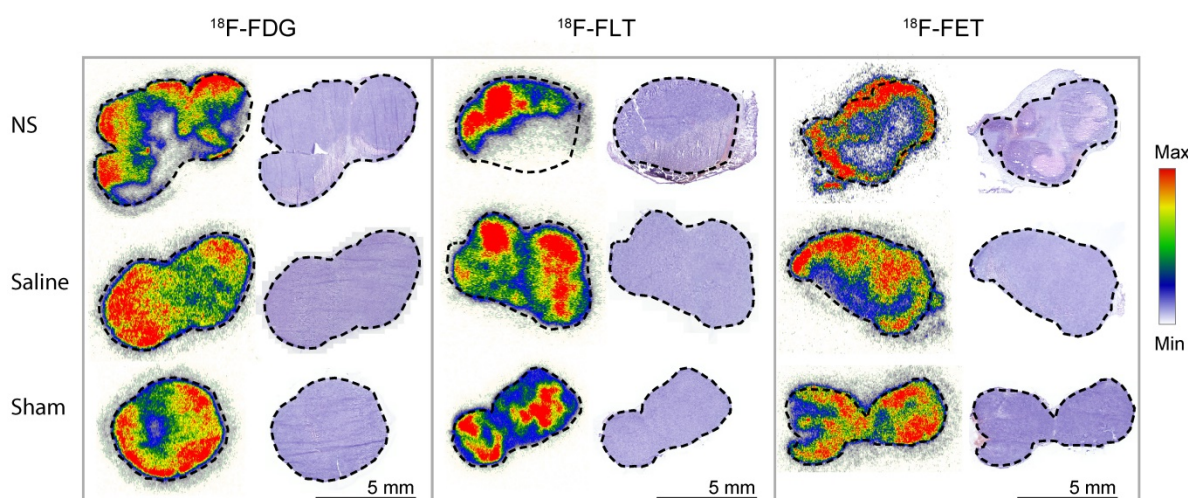


**Figure 6:** Autoradiography and H&E staining. Tissue sections of tumors from each of the treatment groups. Marked-up line represents the border of the tumor. On the left side, the intratumoral distribution of the representative PET tracer is shown and on the right side, the corresponding H&E staining. Each autoradiography image is scaled to its minimum and maximum value.

### Autoradiography and histological analysis of intratumoral tracer uptake

For all three PET tracers, the intratumoral distribution was analyzed by autoradiography two days after photothermal therapy in tumors from each treatment group. For each tumor, the tracer accumulation was compared to hematoxylin and eosin (H&E) staining (see Figure 6). In NS-treated tumors, highly reduced tracer uptake was found to correlate with areas of extensive tumor necrosis. From analysis of the tumors in the control groups, it was evident that the laser or the NS in itself did not cause significant damage to create large areas of necrosis. However, as expected for tumors when they reach a certain size, a small degree of central necrosis was also sometimes observed.

### Discussion

Photothermal cancer therapy using light-absorbing nanoparticles as local heat transducers offers high specificity and has been shown to be effective in many different cancer models in animals, while causing minimal side effects [6, 10, 30-34]. The selection of nanoparticles that fulfill requirements for efficient treatment, e.g., high light-to-heat conversion, EPR-suitable sizes, and biocompatibility, is vast and a result of the effort that has been put into developing nanoparticles since the therapy was first introduced [37]. To move the development of this therapy forward and towards clinical translation, protocols for efficacy assessment and optimization are needed. For this, non-invasive diagnostic modalities are of great value as they allow longitudinal tracking of the outcome of therapy, meanwhile providing early treatment evaluation that

potentially could aid stratifying patients into responders and non-responders [10, 38-40]

Motivated by this, we have in the current study investigated the use of PET/CT imaging for early evaluation of NS-mediated photothermal therapy in mice bearing subcutaneous murine colorectal tumors. We used  $^{18}\text{F}$ -FDG,  $^{18}\text{F}$ -FLT, and  $^{18}\text{F}$ -FET that are imaging glucose uptake, cell proliferation, and amino acid transport, respectively.  $^{18}\text{F}$ -FDG is undoubtedly the most successfully used PET tracer in cancer imaging; however, in some tissues the natural high glucose consumption can prevent its use [11]. Therefore, we also wanted to investigate the use of  $^{18}\text{F}$ -FLT and  $^{18}\text{F}$ -FET as they may have higher specificity for applications where  $^{18}\text{F}$ -FDG is ruled out; or even perform better than  $^{18}\text{F}$ -FDG overall. Finally, we examined if any of them could be used to predict long-term treatment outcome. As the three tracers target different cellular pathways, the treatment response might differ especially in the viable cells in the rim of the ablated area. For example,  $^{18}\text{F}$ -FLT uptake could be affected more than the other two tracers by changes leading to cell cycle arrest. Also, because cancer treatments often induce an inflammatory response, tracers less prone to accumulate in inflammatory lesions, such as  $^{18}\text{F}$ -FET, might have a higher specificity [41].

On the baseline scans we found that all tracers had a fairly high and homogeneous tumor uptake, with only  $^{18}\text{F}$ -FLT showing slightly higher variations than the other two tracers. The benefit of this is that the groups can easily be compared and that a markedly reduction in uptake after therapy can be a robust measure of treatment effect. In all three substudies, photothermal therapy resulted in inhibited tumor growth and overall prolonged

survival compared to control treated animals. We found that after photothermal therapy,  $^{18}\text{F}$ -FDG was on average reduced to 52% of its baseline value in the tumors treated with NS and laser irradiation. In comparison,  $^{18}\text{F}$ -FLT and  $^{18}\text{F}$ -FET were both reduced to 41% of their baseline value, whereas for all three tracers the uptake in the control groups was not significantly changed on day 2. Treatment-induced inflammation could explain why the reduction in  $^{18}\text{F}$ -FDG was slightly smaller compared to the other two tracers. The reduction in uptake in treated areas was confirmed by comparing tracer accumulation in tissue sections measured by autoradiography and H&E staining. It was found that areas of the treated tumors with low tracer uptake coincided with extensive necrotic regions induced by therapy.

Overall, the pronounced reductions in tumor uptake after treatment of all three tracers verify that PET imaging can be used to evaluate the treatment response early after therapy. Somewhat surprisingly, the observed responses from all three tracers were at large similar, suggesting that the major contribution in imaging signal stems from the ablated region where all cells are necrotic. Moreover, to see if the relative change in uptake held information on tumor growth following therapy we investigated the relationship between the uptake ratio (day 2/baseline) and survival for all animals in the studies. We found that tumors with high reduction in uptake at day 2 were also the tumors where the treatment effect was best and the animals lived longest. In particular  $^{18}\text{F}$ -FDG had a strong linear relationship between change in uptake and overall survival, while the correlation was moderate for  $^{18}\text{F}$ -FLT and weak for  $^{18}\text{F}$ -FET. As glucose is essential for energy production, more or less all viable cells will have a continuously basal uptake of  $^{18}\text{F}$ -FDG, whereas  $^{18}\text{F}$ -FLT and  $^{18}\text{F}$ -FET accumulation will be more prone to fluctuations dependent on the physiological state of the cells. Overall these results suggest that for this application,  $^{18}\text{F}$ -FDG may be a better prognostic marker than  $^{18}\text{F}$ -FLT and  $^{18}\text{F}$ -FET.

In each of the NS-treated groups, there were animals with complete tumor regression, however, most animals experienced tumor relapse. Although this was beyond the scope of this study, we believe that the treatment response can be optimized by, e.g., exposure of higher laser intensity, multiple laser irradiations, or combination therapy for synergistic effects. For the purpose of optimizing the therapy, PET imaging would be a highly valuable tool where the tumor uptake early after therapy could be used to determine if the response was as desired or otherwise direct an early change to a strategy that could improve the patient's outcome.

## Conclusion

In this study we found that both  $^{18}\text{F}$ -FDG,  $^{18}\text{F}$ -FLT, and  $^{18}\text{F}$ -FET can be used for early non-invasive evaluation of photothermal cancer therapy already two days after treatment. Although  $^{18}\text{F}$ -FDG holds the strongest prognostic information in this study, this could vary between tumor models. The robustness of all three tracers in terms of treatment response suggests that the most appropriate tracer can be freely selected without loss of information relative to the other PET tracers. In conclusion, PET imaging using  $^{18}\text{F}$ -FDG,  $^{18}\text{F}$ -FLT, or  $^{18}\text{F}$ -FET, all commonly used in a clinical setting, are reliable methods for evaluation and optimization of nanoparticle-assisted photothermal therapy and shows promise for personalizing therapy.

## Acknowledgement

Financial support from the Novo Nordisk Foundation, the Lundbeck Foundation, Innovation Fund Denmark, the Svend Andersen Foundation, the Arvid Nilsson Foundation, the John and Birthe Meyer Foundation, the Research Foundation of Rigshospitalet, the Research Foundation of the Capital Region, the Global Excellence Program, H2020 program and ERC advanced grant are gratefully acknowledged.

## Competing Interests

The authors have declared that no competing interest exists.

## References

- Chen J, Glaus C, Laforest R, Zhang Q, Yang M, Gidding M, et al. Gold nanocages as photothermal transducers for cancer treatment. *Small*. 2010; 6: 811-7.
- Dickerson EB, Dreaden EC, Huang X, El-Sayed IH, Chu H, Pushpanketh S, et al. Gold nanorod assisted near-infrared plasmonic photothermal therapy (PPTT) of squamous cell carcinoma in mice. *Cancer Lett*. 2008; 269: 57-66.
- Hirsch LR, Stafford RJ, Bankson JA, Sershen SR, Rivera B, Price RE, et al. Nanoshell-mediated near-infrared thermal therapy of tumors under magnetic resonance guidance. *Proc Natl Acad Sci U S A*. 2003; 100: 13549-54.
- Huang N, Wang H, Zhao J, Lui H, Korbelik M, Zeng H. Single-wall carbon nanotubes assisted photothermal cancer therapy: animal study with a murine model of squamous cell carcinoma. *Lasers Surg Med*. 2010; 42: 638-48.
- Moon HK, Lee SH, Choi HC. In vivo near-infrared mediated tumor destruction by photothermal effect of carbon nanotubes. *ACS Nano*. 2009; 3: 3707-13.
- O'Neal DP, Hirsch LR, Halas NJ, Payne JD, West JL. Photo-thermal tumor ablation in mice using near infrared-absorbing nanoparticles. *Cancer Lett*. 2004; 209: 171-6.
- Eisenhauer EA, Therasse P, Bogaerts J, Schwartz LH, Sargent D, Ford R, et al. New response evaluation criteria in solid tumours: revised RECIST guideline (version 1.1). *Eur J Cancer*. 2009; 45: 228-47.
- Wahl RL, Jacene H, Kasamon Y, Lodge MA. From RECIST to PERCIST: Evolving Considerations for PET response criteria in solid tumors. *J Nucl Med*. 2009; 50 Suppl 1: 122S-50S.
- Pauwels EK, Ribeiro MJ, Stoot JH, McCready VR, Bourguignon M, Maziere B. FDG accumulation and tumor biology. *Nucl Med Biol*. 1998; 25: 317-22.
- Norregaard K, Jorgensen JT, Simon M, Melander F, Kristensen LK, Bendix PM, et al.  $^{18}\text{F}$ -FDG PET/CT-based early treatment response evaluation of nanoparticle-assisted photothermal cancer therapy. *PLoS One*. 2017; 12: e0177997.
- Bakheet SM, Powe J. Benign causes of  $^{18}\text{F}$ -FDG uptake on whole body imaging. *Semin Nucl Med*. 1998; 28: 352-8.

12. Long NM, Smith CS. Causes and imaging features of false positives and false negatives on F-PET/CT in oncologic imaging. *Insights Imaging*. 2011; 2: 679-98.
13. Galban CJ, Bhojani MS, Lee KC, Meyer CR, Van Dort ME, Kuszpit KK, et al. Evaluation of treatment-associated inflammatory response on diffusion-weighted magnetic resonance imaging and 2-[18F]-fluoro-2-deoxy-D-glucose-positron emission tomography imaging biomarkers. *Clin Cancer Res*. 2010; 16: 1542-52.
14. Bednarova S, Lindenberg ML, Vinsensia M, Zuiani C, Choyke PL, Turkbey B. Positron emission tomography (PET) in primary prostate cancer staging and risk assessment. *Transl Androl Urol*. 2017; 6: 413-23.
15. Galldiks N, Law I, Pope WB, Arbizu J, Langen KJ. The use of amino acid PET and conventional MRI for monitoring of brain tumor therapy. *Neuroimage Clin*. 2017; 13: 386-94.
16. Avril S, Muzic RF, Jr., Plecha D, Traughber BJ, Vinayak S, Avril N. (1)(8)F-FDG PET/CT for Monitoring of Treatment Response in Breast Cancer. *J Nucl Med*. 2016; 57 Suppl 1: 34S-9S.
17. O JH, Choi WH, Han EJ, Choi EK, Chae BJ, Park YG, et al. The Prognostic Value of (18)F-FDG PET/CT for Early Recurrence in Operable Breast Cancer: Comparison with TNM Stage. *Nucl Med Mol Imaging*. 2013; 47: 263-7.
18. Shields AF, Grierson JR, Dohmen BM, Machulla HJ, Stayanoff JC, Lawhorn-Crews JM, et al. Imaging proliferation in vivo with [F-18]FLT and positron emission tomography. *Nat Med*. 1998; 4: 1334-6.
19. Been LB, Suurmeijer AJ, Cobben DC, Jager PL, Hoekstra HJ, Elsinga PH. [18F]FLT-PET in oncology: current status and opportunities. *Eur J Nucl Med Mol Imaging*. 2004; 31: 1659-72.
20. Rasey JS, Grierson JR, Wiens LW, Kolb PD, Schwartz JL. Validation of FLT uptake as a measure of thymidine kinase-1 activity in A549 carcinoma cells. *J Nucl Med*. 2002; 43: 1210-7.
21. Wester HJ, Herz M, Weber W, Heiss P, Senekowitsch-Schmidtke R, Schwaiger M, et al. Synthesis and radiopharmacology of O-(2-[18F]fluoroethyl)-L-tyrosine for tumor imaging. *J Nucl Med*. 1999; 40: 205-12.
22. Langen KJ, Stoffels G, Filss C, Heinzel A, Stegmayr C, Lohmann P, et al. Imaging of amino acid transport in brain tumours: Positron emission tomography with O-(2-[18F]fluoroethyl)-L-tyrosine (FET). *Methods*. 2017; 130: 124-34.
23. Heiss P, Mayer S, Herz M, Wester HJ, Schwaiger M, Senekowitsch-Schmidtke R. Investigation of transport mechanism and uptake kinetics of O-(2-[18F]fluoroethyl)-L-tyrosine in vitro and in vivo. *J Nucl Med*. 1999; 40: 1367-73.
24. Jorgensen JT, Norregaard K, Tian P, Bendix PM, Kjaer A, Oddershede LB. Single Particle and PET-based Platform for Identifying Optimal Plasmonic Nano-Heaters for Photothermal Cancer Therapy. *Sci Rep*. 2016; 6: 30076.
25. Pang B, Zhao Y, Luehmann H, Yang X, Detering L, You M, et al. (6)(4)Cu-Doped PdCu@Au Tripods: A Multifunctional Nanomaterial for Positron Emission Tomography and Image-Guided Photothermal Cancer Treatment. *ACS Nano*. 2016; 10: 3121-31.
26. Wang Y, Black KC, Luehmann H, Li W, Zhang Y, Cai X, et al. Comparison study of gold nanohexapods, nanorods, and nanocages for photothermal cancer treatment. *ACS Nano*. 2013; 7: 2068-77.
27. [Internet] Pilot Study of AuroLase(tm) Therapy in Refractory and/or Recurrent Tumors of the Head and Neck. <https://clinicaltrials.gov/ct2/show/NCT00848042>.
28. [Internet] MRI/US Fusion Imaging and Biopsy in Combination With Nanoparticle Directed Focal Therapy for Ablation of Prostate Tissue. <https://clinicaltrials.gov/ct2/show/NCT02680535>.
29. [Internet] Efficacy Study of AuroLase Therapy in Subjects With Primary and/or Metastatic Lung Tumors. <https://clinicaltrials.gov/ct2/show/NCT01679470>.
30. Ayala-Orozco C, Urban C, Knight MW, Urban AS, Neumann O, Bishnoi SW, et al. Au nanomatryoshkas as efficient near-infrared photothermal transducers for cancer treatment: benchmarking against nanoshells. *ACS Nano*. 2014; 8: 6372-81.
31. Day ES, Thompson PA, Zhang L, Lewinski NA, Ahmed N, Drezek RA, et al. Nanoshell-mediated photothermal therapy improves survival in a murine glioma model. *J Neurooncol*. 2011; 104: 55-63.
32. Xie H, Wang ZJ, Bao A, Goins B, Phillips WT. In vivo PET imaging and biodistribution of radiolabeled gold nanoshells in rats with tumor xenografts. *Int J Pharm*. 2010; 395: 324-30.
33. Stern JM, Stanfield J, Kabbani W, Hsieh JT, Cadeddu JA. Selective prostate cancer thermal ablation with laser activated gold nanoshells. *J Urol*. 2008; 179: 748-53.
34. Bardhan R, Chen W, Bartels M, Perez-Torres C, Botero MF, McAninch RW, et al. Tracking of multimodal therapeutic nanocomplexes targeting breast cancer in vivo. *Nano Lett*. 2010; 10: 4920-8.
35. Stern JM, Kibanov Solomonov VV, Sazykina E, Schwartz JA, Gad SC, Goodrich GP. Initial Evaluation of the Safety of Nanoshell-Directed Photothermal Therapy in the Treatment of Prostate Disease. *Int J Toxicol*. 2016; 35: 38-46.
36. Gad SC, Sharp KL, Montgomery C, Payne JD, Goodrich GP. Evaluation of the toxicity of intravenous delivery of auroshell particles (gold-silica nanoshells). *Int J Toxicol*. 2012; 31: 584-94.
37. Jaque D, Martinez Maestro L, del Rosal B, Haro-Gonzalez P, Benayas A, Plaza JL, et al. Nanoparticles for photothermal therapies. *Nanoscale*. 2014; 6: 9494-530.
38. Fu G, Zhu L, Yang K, Zhuang R, Xie J, Zhang F. Diffusion-Weighted Magnetic Resonance Imaging for Therapy Response Monitoring and Early Treatment Prediction of Photothermal Therapy. *ACS Appl Mater Interfaces*. 2016; 8: 5137-47.
39. Zhang F, Cao J, Chen X, Yang K, Zhu L, Fu G, et al. Noninvasive Dynamic Imaging of Tumor Early Response to Nanoparticle-mediated Photothermal Therapy. *Theranostics*. 2015; 5: 1444-55.
40. Jin CS, Overchuk M, Cui L, Wilson BC, Bristow RG, Chen J, et al. Nanoparticle-Enabled Selective Destruction of Prostate Tumor Using MRI-Guided Focal Photothermal Therapy. *Prostate*. 2016; 76: 1169-81.
41. Rau FC, Weber WA, Wester HJ, Herz M, Becker I, Kruger A, et al. O-(2-[18F]fluoroethyl)-L-tyrosine (FET): a tracer for differentiation of tumour from inflammation in murine lymph nodes. *Eur J Nucl Med Mol Imaging*. 2002; 29: 1039-46.